Na, K-ATPase α3 is a death target of Alzheimer patient amyloid-β assembly

Takayuki Ohnishi[a,b,1], Masako Yanazawa[c,1], Tomoya Sasahara[a,b], Yasuki Kitamura[c], Hidekazu Hiroaki[d], Yugo Fukazawa[e], Isao Kii[f], Takashi Nishiyama[a,f], Akiyoshi Kakita[g], Hiroyuki Takeda[h], Akihide Takeuchi[f], Yoshie Arai[a,b], Akane Ito[c,2], Hitomi Komura[a,b], Hajime Hirao[i], Kaori Satomura[a,b], Masafumi Inoue[a,b], Shin-ichi Muramatsu[j], Ko Matsui[k], Mari Tada[g], Michio Sato[c,3], Eri Saijo[a,b], Yoshiki Shigemitsu[d], Satoko Sakai[a,b], Yoshitaka Umetsu[d], Natsuko Goda[d], Naomi Takino[b], Hitoshi Takahashi[g], Masatoshi Hagiwara[f], Tatsuya Sawasaki[h], Genji Iwasaki[l], Yu Nakamura[m], Yo-ichi Nabeshima[a], David B. Teplow[n], and Minako Hoshi[a,c,f,4]

[a]Institute of Biomedical Research and Innovation, Foundation for Biomedical Research and Innovation (FBRI), Kobe 650-0047, Japan; [b]TAO Health Life Pharma Co. Ltd. (TAO), Medical Innovation Center in Kyoto University, Kyoto 606-8507, Japan; [c]Mitsubishi Kagaku Institute of Life Sciences (MITILS; dissolved in March 2010); [d]Department of Basic Medicinal Sciences, Graduate School of Pharmaceutical Sciences, Nagoya University, Nagoya 464-8601, Japan; [e]Department of Histological and Physiological Sciences, Faculty of Medical Science, University of Fukui, Yoshida 910-1193, Japan; [f]Department of Anatomy and Developmental Biology, Graduate School of Medicine, Kyoto University, Kyoto 606-8501, Japan; [g]Department of Pathology, Brain Research Institute, Niigata University, Niigata 951-8585, Japan; [h]Proteo-Science Center, Ehime University, Matsuyama 790-8577, Japan; [i]School of Physical and Mathematical Sciences, Nanyang Technological University, Singapore 637371; [j]Department of Medicine, Jichi Medical University, Shimotsuke 329-0498, Japan; [k]Division of Interdisciplinary Medical Science, Graduate School of Medicine, Tohoku University, Sendai 980-8575, Japan; [l]Faculty of Pharmacy, Takasaki University of Health and Welfare, Takasaki 370-0033, Japan; [m]Department of Neuropsychiatry, Faculty of Medicine, Kagawa University, Kagawa 761-0793, Japan; and [n]Department of Neurology, David Geffen School of Medicine, University of California, Los Angeles, CA 90095

Edited by Thomas C. Südhof, Stanford University School of Medicine, Stanford, CA, and approved July 6, 2015 (received for review November 6, 2014)

Neurodegeneration correlates with Alzheimer's disease (AD) symptoms, but the molecular identities of pathogenic amyloid β-protein (Aβ) oligomers and their targets, leading to neurodegeneration, remain unclear. Amylospheroids (ASPD) are AD patient-derived 10- to 15-nm spherical Aβ oligomers that cause selective degeneration of mature neurons. Here, we show that the ASPD target is neuron-specific Na^+/K^+-ATPase α3 subunit (NAKα3). ASPD-binding to NAKα3 impaired NAKα3-specific activity, activated N-type voltage-gated calcium channels, and caused mitochondrial calcium dyshomeostasis, tau abnormalities, and neurodegeneration. NMR and molecular modeling studies suggested that spherical ASPD contain N-terminal-Aβ–derived "thorns" responsible for target binding, which are distinct from low molecular-weight oligomers and dodecamers. The fourth extracellular loop (Ex4) region of NAKα3 encompassing Asn^{879} and Trp^{880} is essential for ASPD–NAKα3 interaction, because tetrapeptides mimicking this Ex4 region bound to the ASPD surface and blocked ASPD neurotoxicity. Our findings open up new possibilities for knowledge-based design of peptidomimetics that inhibit neurodegeneration in AD by blocking aberrant ASPD–NAKα3 interaction.

NMR | computational modeling | abnormal protein–protein interaction in synapse | hyperexcitotoxicity | protein–protein interaction inhibitors

Alzheimer's disease (AD) brains characteristically display fibrillar and nonfibrillar (oligomeric) protein assemblies composed of the amyloid β-protein (Aβ) (1–6). Aβ has been shown to bind to postsynaptic receptors, such as α7-nicotinic acetylcholine receptor (α7nAChR) (7), receptor for advanced glycation end products (RAGE) (8), receptor tyrosine kinase EPHB2 (9), and cellular prion protein PrP^C (10). These "Aβ receptors," except for RAGE, have been reported to mediate toxicity of Aβ oligomers through modulating NMDA receptors (NMDAR) (11). Aβ oligomers, including dimers from AD brains (12, 13), dodecamers (Aβ*56) from AD model mice (14), and in vitro-generated Aβ-derived diffusible ligands (ADDLs) (15, 16), induce synaptic impairment by affecting NMDAR (11). Thus, NMDAR are a common target for synaptic impairment in AD. However, these oligomers do not cause neuronal death (12, 14). The atomic resolution structures of neurotoxic Aβ oligomers and their in vivo targets leading to neuronal death in AD remain unclear (6), even though neuronal death is the central mechanism responsible for symptomatic onset in AD (17).

We previously isolated neurotoxic Aβ oligomers, termed amylospheroids (ASPD), from the brains of AD patient (18–20). ASPD appear in transmission electron microscopic (TEM) images as spheres of diameter ~11.9 ± 1.7 nm (19). ASPD appear to be unique Aβ assemblies, as determined immunochemically. These structures are recognized strongly by ASPD-specific antibodies (K_d ~ pM range), but not with the oligomer-specific polyclonal antiserum A11 (19). ASPD are distinct from Aβ dimers, ADDLs, dodecamers, and other A11-reactive entities (19).

ASPD cause severe degeneration of mature human neurons (19). ASPD levels in the cortices of AD patients correlate well

Significance

Alzheimer's disease (AD) involves neuron dysfunction and loss. This brain damage is thought to be caused by a small protein, the amyloid β-protein (Aβ), which forms aggregates that are neurotoxic. This neurotoxicity has been explained by multiple mechanisms. We reveal here a new neurotoxic mechanism that involves the interaction between patient-derived Aβ assemblies, termed amylospheroids, and the neuron-specific Na^+/K^+-ATPase α3 subunit. This interaction causes neurodegeneration through presynaptic calcium overload, which explains earlier observations that such neuronal hyperactivation is an early indicator of AD-related neurodegeneration. Importantly, amylospheroid concentrations correlate with disease severity and progression in AD patients. Amylospheroid:neuron-specific Na^+/K^+-ATPase α3 subunit interactions may be a useful therapeutic target for AD.

Author contributions: H. Hiroaki, Y.F., I.K., D.B.T., and M. Hoshi designed research; T.O., M.Y., T. Sasahara, Y.K., T.N., H. Takeda, A.T., Y.A., A.I., H.K., H. Hirao, K.S., M.I., M.T., M.S., E.S., Y.S., S.S., Y.U., N.G., N.T., and M. Hoshi performed research; T.O., M.Y., T. Sasahara, Y.K., H. Hiroaki, Y.F., I.K., T.N., A.K., H. Takeda, A.T., Y.A., A.I., H.K., H. Hirao, K.S., M.I., S.-i.M., K.M., M.T., M.S., E.S., Y.S., S.S., Y.U., N.G., N.T., H. Takahashi, M. Hagiwara, T. Sawasaki, G.I., Y.N., Y.-i.N., D.B.T., and M. Hoshi analyzed data; and H. Hiroaki, Y.F., I.K., D.B.T., and M. Hoshi wrote the paper.

Conflict of interest statement: M. Hoshi has served as a technical advisor to TAO, a Kyoto University-derived bioventure, with the permission of the conflict-of-interest committee of Kyoto University. T. Sasahara, Y.A., H.K., K.S., M.I., E.S., S.S., and N.T. are employees of TAO.

This article is a PNAS Direct Submission.

Freely available online through the PNAS open access option.

[1]T.O. and M.Y. contributed equally to this work.

[2]Present address: Institute of Industrial Science, University of Tokyo, Tokyo 153-8505, Japan.

[3]Present address: Graduate School of Agriculture, Meiji University, Kawasaki 214-8571, Japan.

[4]To whom correspondence should be addressed. Email: hoshi.minako.8w@kyoto-u.ac.jp.

This article contains supporting information online at www.pnas.org/lookup/suppl/doi:10.1073/pnas.1421182112/-/DCSupplemental.

with disease severity (19). In contrast, ASPD-like oligomers were minimally detectable in the brains of transgenic mice expressing human amyloid precursor protein (*APP*), in which no significant neuronal loss is observed (19). These findings suggest that ASPD are an important effector of neuronal death in AD patients. We sought to elucidate mechanisms of ASPD-induced neurotoxicity. We report here that ASPD interact with the α-subunit of neuron-specific Na^+/K^+-ATPase (NAKα3), resulting in presynaptic calcium overload and neuronal death.

Results

ASPD Bind To NAKα3 In Mature Neurons. ASPD caused degeneration of mature rat hippocampal neurons, but not immature neurons or nonneuronal HEK293 (Fig. 1*A*). ASPD toxicity required binding to mature neurons, because ASPD-specific mouse monoclonal amylospheroid (mASD)3 antibody blocked binding and toxicity of ASPD (Fig. 1 *A* and *B*). [The K_d for ASPD binding = 5.43 ± 0.27 nM (n = 3) (Fig. 1*C*). ASPD concentration was determined using an average ASPD molecular weight of 128 kDa (20). See summary of the characteristics of patient and synthetic ASPD in Table S1. See also *SI Discussion* for an updated definition of ASPD.] Blockers of known Aβ receptors (21), including glutamate receptors (NMDA, non-NMDA, and metabotropic types) and voltage-gated sodium channels, did not affect ASPD neurotoxicity (Fig. S1). These findings suggested ASPD exert their toxicity through binding to novel cell-surface molecules specific to mature neurons.

To identify ASPD-binding proteins on mature neurons, Far-Western ligand-binding assays were performed in a physiological medium. We used ASPD isolated (19) from the soluble brain extracts of the two AD patients displaying the most severe neurodegeneration and the highest ASPD concentrations among those shown in Fig. 2*A* (Fig. 2*B*). These ASPD were A11-negative (Fig. 2*C*), composed predominantly of $Aβ_{1–42}$ and $Aβ_{1–40}$

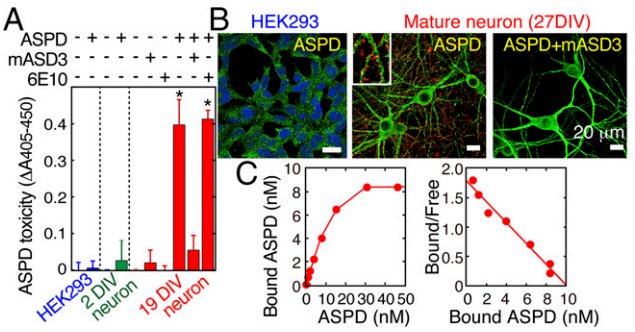

Fig. 1. Mature neuron-specific binding and toxicity of ASPD. (*A*) ASPD neurotoxicity was determined by measuring apoptotic DNA fragmentation in HEK293 cells, 2 DIV immature or 19 DIV mature rat hippocampal neurons after overnight treatment with 140 nM synthetic ASPD, with or without 2-h pretreatment of ASPD with each antibody (0.1 mg/mL for ASPD-specific mASD3 antibody; 0.4 mg/mL for $Aβ_{3–8}$ antibody 6E10) (mean ± SD; *P < 0.001 Games–Howell post hoc test, n = 6). The antibody remained during overnight incubation with ASPD. As shown previously (19), mASD3 inhibited ASPD-induced neuronal death, but 6E10, targeting $Aβ_{3–8}$, did not. ASPD concentration is expressed in terms of the average ASPD mass 128 kDa (20). (*B*) Cells were treated for 30 min with 140 nM synthetic ASPD as in *A*. Images are representative of ASPD binding detected by mASD3 (red). Green represents anti-actin for HEK293 or anti-MAP2 for neurons. Neuronal 2D images were made from the z stack to show neurites (19). Neurons (19–27 DIV) gave essentially the same results as to binding and toxicity of ASPD. (*C*) Binding of synthetic ASPD was performed as in *B*, quantified (10), and shown as ASPD concentrations in 400 μL per well. Scatchard analysis gave K_d = 5.43 ± 0.27 nM (n = 3). B_{max} of ASPD binding was 8.00 ± 1.0 nM for 30 min, from which the maximum level of ASPD binding was calculated to be 14 ± 0.7 pmol of ASPD/mg membrane protein.

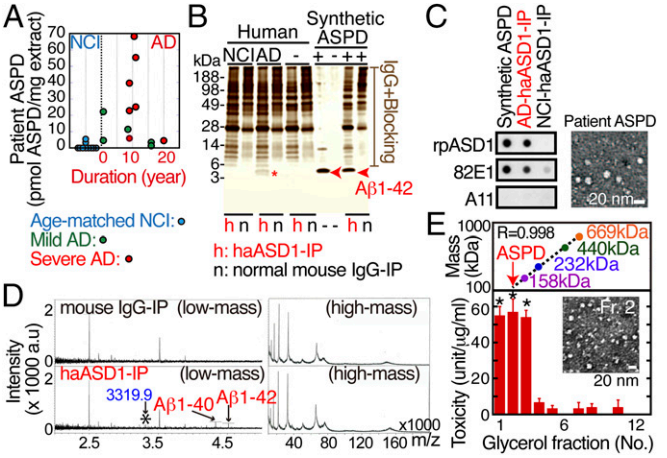

Fig. 2. Characterization of AD patient-derived ASPD. (*A*) Levels of ASPD in soluble extracts of the cerebral cortex are shown according to disease duration and the level of neurodegeneration (see *SI Materials and Methods, Human Brain Pathology and ISH*; reanalysis of the samples used as in ref. 19). ASPD are undetectable in most of the age-matched NCI cases, but are present even in the very early AD cases. ASPD levels in patients increase markedly in parallel with the severity and progression of the disease. The 100-kDa retentates of the extracts from the two patients containing the highest level of ASPD were used for isolation of patient ASPD in this study. In a severe AD patient 20 y after onset, ASPD levels were very low, likely because such widespread neuronal death already had occurred. (*B–D*) Synthetic ASPD and patient ASPD (see above in *A*) were purified by IP using ASPD-specific haASD1 antibody as in ref. 19. Soluble extracts from NCI brains and normal mouse IgG were used as controls for patient extracts and haASD1 antibody, respectively. Silver staining in *B*, dot blotting (*SI Materials and Methods*) along with a TEM image of negatively stained patient ASPD (see *SI Materials and Methods, TEM* for particle analysis) in *C*, and MALDI-TOF/MS analyses in *D* were performed as per ref. 19. Representative data are shown. In the silver-stained gels, a band corresponding to $Aβ_{1–42}$ or $Aβ_{1–40}$ (red asterisk) was detected only in haASD1-immunoislated patient ASPD. Consistently, in MS of patient ASPD, significant peaks corresponding to $Aβ_{1–40}$ (4331.3 Da, centroid) and $Aβ_{1–42}$ (4515.5 Da, centroid) were reproducibly detected. Less-intense peaks at lower mass than $Aβ_{1–40}$ (e.g., see the asterisk in *D*, *Lower Left*) were occasionally, but not reproducibly, detected. The mass of the peak (3319.9 Da, centroid) is consistent with that of [pyroglutamyl-$Aβ_{11–42}$ + H]$^+$. Peaks at higher mass than $Aβ_{40}$ or $Aβ_{42}$ monomer were not detected (*Right*). These findings showed that $Aβ_{1–40}$ and $Aβ_{1–42}$ are the predominant components of patient ASPD. (*E*) Fractionation of patient ASPD (~16 pmol) in a 15–30% linear glycerol gradient (see *SI Materials and Methods, Glycerol Gradient Sedimentation*) (18). Protein standards (aldolase, 158 kDa; catalase, 232 kDa; ferritin, 440 kDa; and thyroglobulin, 669 kDa) were centrifuged at the same time as a reference and used for molecular mass determination (*Upper*). Fractions were collected and immediately assayed for neurotoxicity (*Lower*) (18). One unit of toxicity induces apoptosis in 1% of cells (see *SI Materials and Methods, Glycerol Gradient Sedimentation*). Data were obtained from three independent experiments and normalized to Aβ concentration (mean ± SD; Scheffé's post hoc test, *P < 0.0001 compared with vehicle alone). *Inset* shows a representative TEM image of the sample recovered in fraction 2 (~11.6 ± 2.2-nm spheres; n = 54).

(Fig. 2 *B* and *D*), had molecular masses of 123 ± 20 kDa (Fig. 2*E*), and appeared as ~11.7 ± 1.6-nm spheres (n = 49) in TEM (Fig. 2*C*), consistent with previous data (18–20). We also used in vitro-reconstituted synthetic ASPD, which share essential characteristics with patient ASPD (19) (Table S1), as an analog.

Binding of ASPD was detected with ASPD-specific hamster monoclonal (haASD)1 antibody [K_d for ASPD ~ 0.5 pM (19)]. ASPD bound to a 105-kDa band in extracts from mature neurons cultured for 21 d in vitro (DIV) (red arrowhead in Fig. 3*A*, *Center*), but not immature 2 DIV neurons or HEK293 cells. This band was also recognized by synthetic ASPD (Fig. S2*A*, red arrow on the left), indicating that ASPD bind directly to this band, because purified synthetic ASPD contained no protein other than ASPD (19).

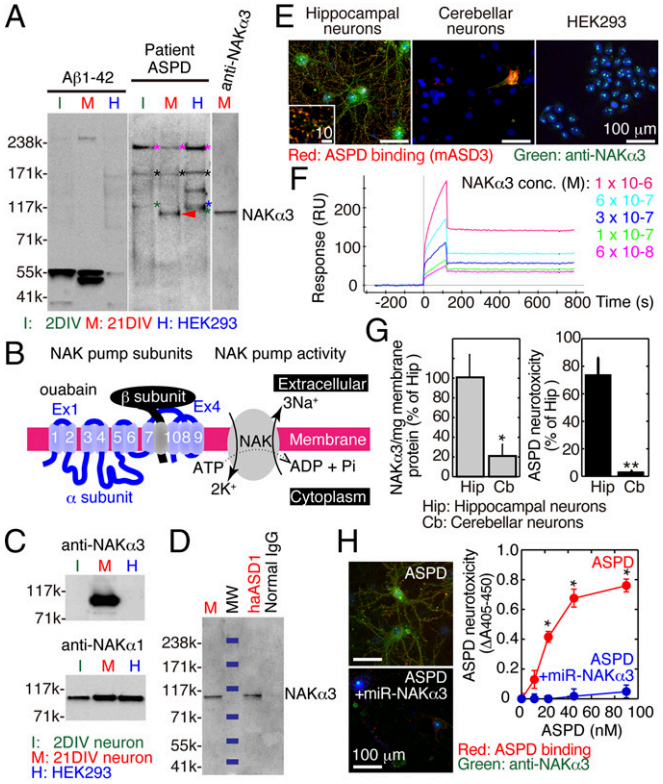

Fig. 3. Patient ASPD bind to NAKα3. (*A*) Far-Western blotting of RIPA extracts (15 μg per lane) was done using 6.6 nM patient ASPD (*Center*; detected with ASPD-specific haASD1 antibody) or 100 nM freshly dissolved $A\beta_{1-42}$ containing monomers and dimers (*Left*; detected with anti-Aβ antibody 6E10). Bands marked with an asterisk represent intracellular proteins (Fig. S2*A*). Western blotting with anti-NAKα3 antibody (excised from *D*) showed the mass of NAKα3 (*Right*). Red arrow indicates a 105-kDa mature neuron-specific ASPD-binding protein, NAKα3. (*B*) Schematic representation of NAK αβ and its function. (*C*) Western blotting of RIPA extracts (used in *A*). (*D*) Coimmunoprecipitation (CoIP) of NAKα3 with 250 nM synthetic ASPD. (*E*) Representative *z*-stack images of 27 DIV hippocampal or 22 DIV cerebellar neurons, or HEK293, treated with 13 nM synthetic ASPD for 15 min. ASPD-binding sites (red) on neuropil colocalize with anti-NAKα3 staining (green) (high-power view in *Inset*; see *SI Materials and Methods, Immunocytochemistry*). (*F*) Direct interaction between ASPD on the tip and rat NAKα3 in micelles using SPR (K_d = 7.8 ± 2.5 nM, n = 3). NAKα3-binding to the tip without ASPD was subtracted as background. NAKβ1 did not interact with ASPD in the AlphaScreen system. (*G*) Rat hippocampal (19–20 DIV) or cerebellar (23 DIV) neurons were treated overnight with 110 nM ASPD. ASPD neurotoxicity was determined as in Fig. 1*A* and normalized to 0.2 μM staurosporine toxicity. NAKα3 levels in membrane fractions of these neurons before ASPD treatment were determined by Western blotting. Mean ± SD; **P* = 0.002; ***P* < 0.0001 compared with hippocampal neurons, n = 3~4 by Scheffé's post hoc test. (*H*) Representative images of 27 DIV hippocampal neurons, with or without selective knockout of NAKα3 (see *SI Materials and Methods, miR of ATP1A3*), treated with 13 nM synthetic ASPD for 15 min. ASPD-binding sites (red) and anti-NAKα3 staining (green) were detected as in *E*. ASPD neurotoxicity was assayed as in Fig. 1*A* (mean ± SD; Scheffé's post hoc test, **P* < 0.0001 compared with vehicle alone, n = 3).

This band was not detected when we used haASD1 alone or synthetic ASPD presaturated with haASD1 (Fig. S2*B*). Unlike ASPD, freshly dissolved $A\beta_{1-42}$, which consisted of monomers, dimers, and other low-molecular-weight (LMW) oligomers, did not bind to the 105-kDa band, but bound to 55-kDa and 45-kDa bands, likely corresponding to 54.2 kDa α7nAChR and 40.4 kDa RAGE, respectively (Fig. 3*A*, *Left*). These findings showed that the 105-kDa band corresponds to ASPD-specific binding proteins present only in mature neurons.

MS and MS/MS analyses of the 105-kDa band (red arrow in Fig. S2*A*, *Right*) identified various NAKα-derived peptides (Table S2). We confirmed that NAKα appeared at 105 kDa (Fig. 3*A*, *Right*). ASPD-binding bands from immature neurons or HEK293 (asterisks in Fig. 3*A*, *Center*, and Fig. S2*A*, *Left*) were identified as intracellular proteins (see legend to Fig. S2*A*). Thus, NAKα, which has a molecular mass of 112–113 kDa, is likely to be the 105-kDa band entity.

NAKα is an essential catalytic subunit of the NAK pump (Fig. 3*B*), which is responsible for keeping the neuron resting membrane potential at about −70 mV (22). The functional NAK pump also requires a β-subunit (22) (Fig. 3*B*). In adult brains, NAKα1 is ubiquitously expressed, whereas NAKα3 is expressed exclusively in neurons, and NAKα2 is found in astrocytes (22). We found that NAKα3 was abundant in extracts of mature neurons only (Fig. 3*C*). Western blotting showed that NAKα3 became detectable at 7 DIV and that its levels continued to increase until 21 DIV in our culture (Fig. S2*C*). This developmental increase in NAKα3 level correlated well with that of the 105-kDa band in Far-Western blotting using synthetic ASPD (Fig. S2*B*). To establish whether NAKα3 is the sole ASPD-binding isoform, we performed coimmunoprecipitation experiments. First, NAKα3 in mature neuron extracts was coimmunoprecipitated directly with purified synthetic ASPD using haASD1 antibody (Fig. 3*D*). Second, biotin-labeled ASPD were incubated with mature hippocampal neurons, and MS/MS analysis confirmed that the NAKα3 isoform was selectively coimmunoprecipitated as the 105-kDa band with biotin-labeled ASPD (red arrows in Fig. S2*D*). We then confirmed that ASPD and NAKα3 were essentially colocalized within the neuropil of mature hippocampal neurons double-stained for synthetic ASPD and NAKα3 (Fig. 3*E*, *Left Inset*). Furthermore, surface plasmon resonance spectroscopy (SPR) demonstrated that rat NAKα3 directly bound to synthetic ASPD (K_d = 7.8 ± 2.5 nM, n = 3) (Fig. 3*F*). The K_d value obtained from this SPR data was almost identical with that obtained from ASPD-binding to mature neurons (Fig. 1*C*) (K_d = 5.43 ± 0.27 nM, as described above). We confirmed that human and mouse NAKα3 bound directly to synthetic ASPD using SPR (human K_d = 28.6 ± 6.6 nM, n = 5; mouse K_d = 4.0 ± 1.9 nM, n = 3). Notably, most mature hippocampal neurons were stained for NAKα3, whereas most mature cerebellar neurons were NAKα3-immunonegative (Fig. S2*E*). This finding was consistent with Western blotting showing that the amount of membrane NAKα3 in cerebellar neurons was only ~20% of that in hippocampal neurons (Fig. 3*G*, *Left*). Synthetic ASPD bound to NAKα3-immunopositive neurons among hippocampal or cerebellar neurons (Fig. 3*E*) and induced death in those neurons at levels correlating with their membrane NAKα3 amount (Fig. 3*G*). Stable knockout of NAKα3 expression with microRNA (miR)-expressing virus vector decreased NAKα3-expressing neurons to 19.8 ± 14% (n = 3; P < 0.0001 compared with the untreated neurons using Scheffé's post hoc test, n = 3) in hippocampal neurons and abolished ASPD-binding and ASPD-induced neurodegeneration (Fig. 3*H*). These data support the conclusion that NAKα3 is the mature neuron-specific ASPD-binding protein that is linked to ASPD neurotoxicity.

ASPD Impair NAKα3 Activity, Leading to Ca^{2+} Dyshomeostasis and Neuron Death. We next examined the effect of ASPD-binding on NAKα3 activity. As shown in Fig. 4*A*, exposure of membrane preparations from mature hippocampal neurons to 110 nM synthetic ASPD rapidly (~70% in 1 h) impaired NAKα3-specific activity in those membrane preparations. Overnight treatment of intact mature hippocampal neurons with 140 nM synthetic ASPD caused a >90% decrease in NAKα3-specific activity (Fig. 4*B*).

This NAKα3 impairment should cause a failure in active transport of Na^+ and K^+ ions (Fig. 3*B*). Indeed, we found that cytoplasmic Na^+ levels were increased immediately after exposure of neurons to synthetic ASPD (at the orange arrow in Fig. S3*A*), which reached a maximum after ~18 min (at the yellow arrow in

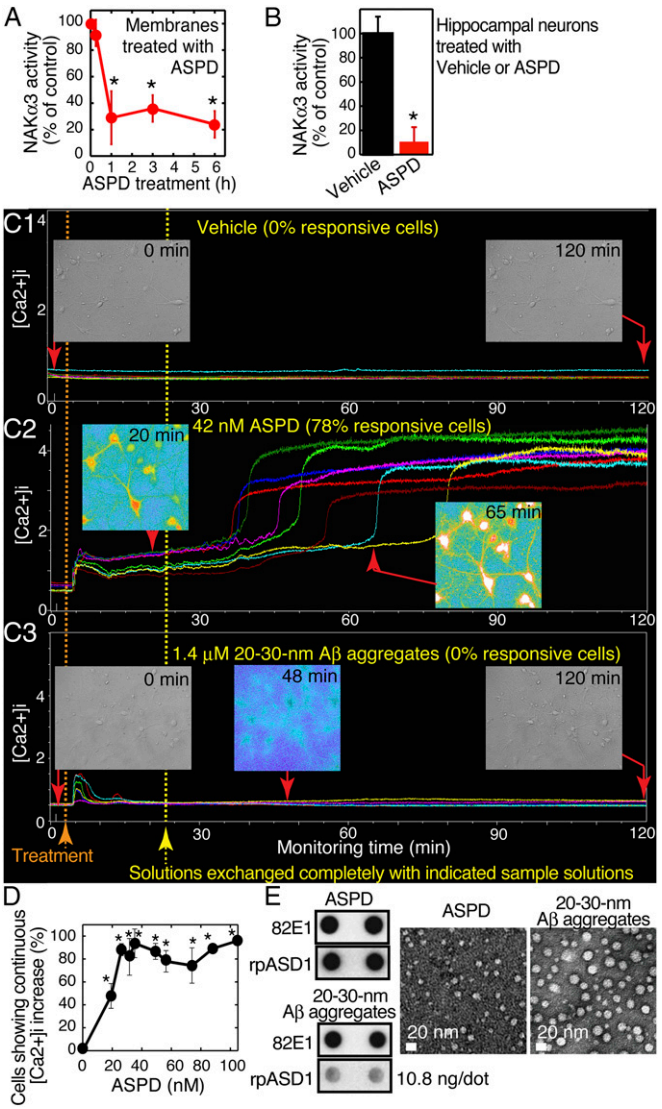

Fig. 4. ASPD impair NAK activity and cause Ca^{2+} dyshomeostasis. (*A*) Membrane fraction of 25–26 DIV hippocampal neurons (30 μg per assay) was incubated with 110 nM synthetic ASPD and NAKα3-specific ATPase activity [K_d = 45 nM for ouabain (61–63)] was determined by subtracting the 100-nM ouabain-sensitive activity from overall Mg^{2+}-ATPase activity (46). Mean ± SD; *$P < 0.0001$ Scheffé's post hoc test compared with 0 h, $n = 4$. (*B*) NAKα3-specific ATPase activity of 25–26 DIV hippocampal neurons treated overnight with 140 nM synthetic ASPD was determined as in *A*. Mean ± SD; *$P < 0.0001$ Scheffé's post hoc test, $n = 3$. (*C*) Representative $[Ca^{2+}]_i$ changes of cell bodies of 19–20 DIV hippocampal neurons after treatment with each sample using Fura-PE3AM. The ratio of responsive cells was obtained as in *D*. The 20- to 30-nm $Aβ_{1–42}$ aggregates were obtained by concentration and redilution processes (see *SI Materials and Methods, Preparation of 20- to 30-nm Aβ Aggregates*). For treatment with ASPD, the circulating buffer was replaced with the buffer containing ASPD. After the replacement, it took ~110 s until the ASPD-containing fluid reached the assay chamber (at the orange arrow) and it took ~17.5 min until all of the solution in the assay chamber was replaced by the ASPD solution (at the yellow arrow). Treatment with 20- to 30-nm $Aβ_{1–42}$ aggregates was done similarly. (*D*) The ratio of neurons that exhibited repetitive Ca^{2+} spikes or reached a saturated $[Ca^{2+}]_i$ within 2 h after the treatment was calculated from $[Ca^{2+}]_i$ data from three independent experiments. Mean ± SD; *$P < 0.0001$ Scheffé's post hoc test. (*E*) TEM images and dot blotting of the samples used in *C*.

Fig. S3 A_3 and A_4). ASPD-induced impairment of NAKα3 activity thus increased cytoplasmic Na^+ levels and likely induced depolarization in the treated neurons.

This process would lead to an increase in intracellular Ca^{2+} level ($[Ca^{2+}]_i$) through the plasma membrane Na^+/Ca^{2+} exchanger (NCX) or voltage-gated Ca^{2+} channels (VGCC) activated by depolarization (22). We therefore monitored $[Ca^{2+}]_i$ using Fura-PE3AM staining. Vehicle treatments did not affect $[Ca^{2+}]_i$ for at least 2 h (Fig. 4*C1* and Fig. S3B_1), but ASPD increased the number of Ca^{2+}-responsive cells dose-dependently (Fig. 4*C2* and Fig. S3 B_2–B_4), with a plateau at ~40 nM synthetic ASPD (Fig. 4*D*). The dose-dependent effect of ASPD on the number of Ca^{2+}-responsive cells correlated well with the level of ASPD-binding (Fig. 1*C*, *Left*), as well as that of ASPD neurotoxicity ($EC_{50} = 18 \pm 2.4$ nM, $n = 5$), suggesting that ASPD-binding to mature neurons caused increased $[Ca^{2+}]_i$, leading to eventual neuronal death.

Depending on the ASPD concentration, two types of Ca^{2+}-responses were observed (see *SI Discussion* for a plausible mechanistic explanation). With 18 nM ASPD, repetitive Ca^{2+} spikes were observed ~3 min after the treatment (Fig. S3B_2). In this case, $[Ca^{2+}]_i$ increased gradually and led to a sustained increase after 2 h (e.g., Fig. S3C_1). With higher concentrations of ASPD (e.g., 42 nM in Fig. 4*C2*), $[Ca^{2+}]_i$ increased ~2 min after the treatment, maintained a sustained increase during 0–40 min, and then rose precipitously before plateauing at ~40–70 min. Much higher concentrations of ASPD accelerated the process, with $[Ca^{2+}]_i$ plateauing earlier (within 1 h; compare 88 nM synthetic ASPD in Fig. S3B_4 with 42 nM synthetic ASPD in Fig. S3B_3). Unlike ASPD, 1.4 μM 20–30-nm $Aβ_{1–42}$ aggregates (TEM in Fig. 4*E*), which were obtained by making a 20-fold concentration and then a 10-fold redilution of ASPD (*SI Materials and Methods, Preparation of 20- to 30-nm Aβ Aggregates*), were rarely detected by ASPD-specific rabbit polyclonal (rpASD)1 antibody in dot blotting (Fig. 4*E*) and did not cause such a persistent increase in $[Ca^{2+}]_i$ (Fig. 4*C3*), and the neurons remained intact (inset bright-field images in Fig. 4*C3*).

This ASPD-induced increase in $[Ca^{2+}]_i$ required extracellular Ca^{2+}, because it was blocked by addition of EGTA to the medium (Fig. S3C_2). Furthermore, blockade of $[Ca^{2+}]_i$ overload by chelation with BAPTA-AM suppressed ASPD toxicity (Fig. 5*A*). We then asked which plasma membrane calcium conductors, VGCC or NCX, were involved in ASPD toxicity. Inhibitor effects on ASPD neurotoxicity showed that N-type VGCC were involved in ASPD-induced neuronal death, whereas the other VGCC subtypes and NCX were not involved (Fig. 5*A*). We confirmed that an inhibitor specific to N-type VGCC blocked ASPD-induced $[Ca^{2+}]_i$ increase (Fig. S3D_3). Notably, N-type VGCC are found primarily at presynaptic terminals of neurons (23), consistent with presynaptic binding of ASPD (19).

Next, we examined whether the two major intracellular Ca^{2+} stores, mitochondria and endoplasmic reticulum (ER), could be involved in ASPD neurotoxicity. A mitochondrial NCX inhibitor and an inhibitor of mitochondrial permeability transition (MPT) pore opening both blocked ASPD-induced apoptosis, whereas an inhibitor of Ca^{2+} influx in ER (mediated by a Ca^{2+} sensor, STIM1), an IP3 receptor antagonist, or a ryanodine receptor (RyR) antagonist, failed to block ASPD neurotoxicity (Fig. 5*A*). Thus, Ca^{2+} dyshomeostasis in mitochondria was involved in ASPD neurotoxicity, but ER Ca^{2+} stores were not (Fig. 5 *A* and *B*). We found that treatment with both CGP37157 (a mitochondrial NCX inhibitor) and cyclosporin A (an inhibitor of mitochondrial MPT pore opening) inhibited the ASPD-induced sharp $[Ca^{2+}]_i$ increase that followed the initial sustained increase in $[Ca^{2+}]_i$ more strongly than the single treatments (Fig. S3*E*). This finding suggests that mitochondrial NCX and MPT pore opening are both involved in Ca^{2+} release from mitochondria that is linked to ASPD neurotoxicity (see Fig. S3*E* for more details).

These findings indicate that impairment of NAKα3 activity by ASPD binding increases cytoplasmic Na^+ levels (Fig. S3*A*), activates N-type VGCC, and causes continuous Ca^{2+} influx into cytoplasm. This in turn results in Ca^{2+} overload in mitochondria (observed as the sustained $[Ca^{2+}]_i$ increase) and subsequent Ca^{2+}

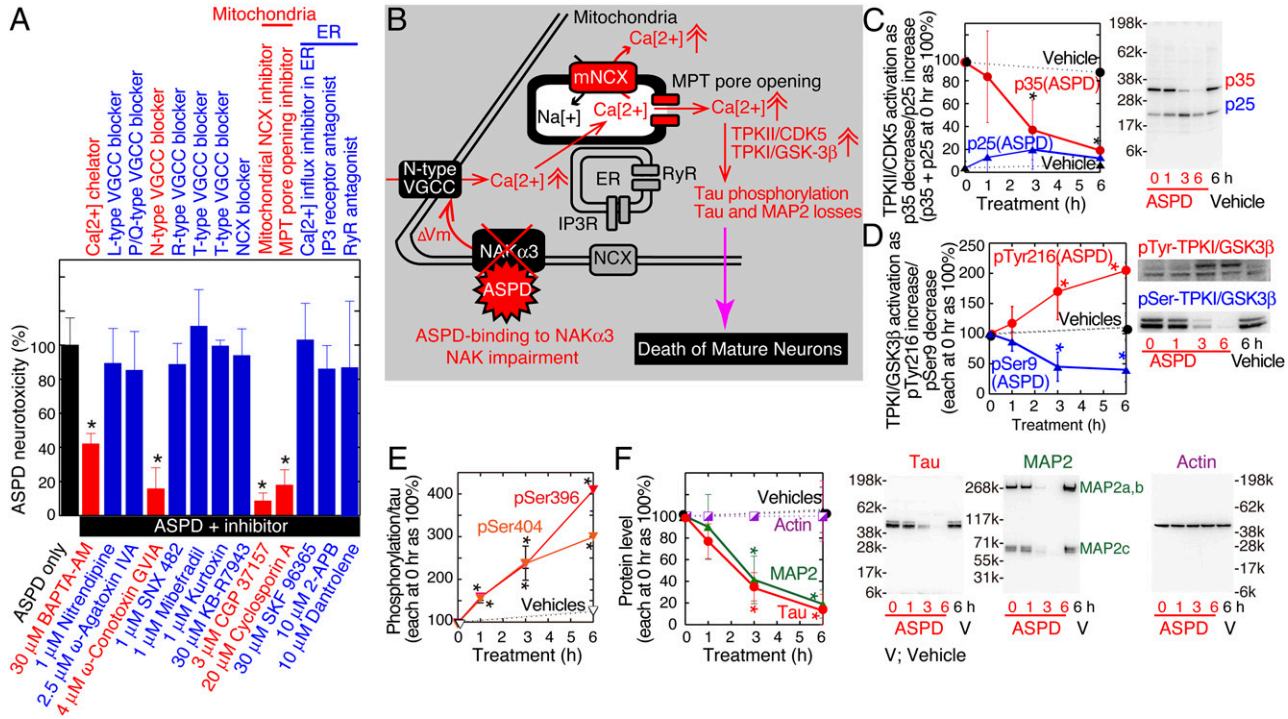

Fig. 5. Downstream signals leading to neuronal death after ASPD binding to NAKα3. (*A*) Inhibitor effect on 140 nM synthetic ASPD neurotoxicity examined as in Fig. 1*A*. Mean ± SD; **P* < 0.001 compared with ASPD only (Scheffé's post hoc test, *n* = 3). (*B*) Schematic illustration of the mechanism of ASPD-induced neurodegeneration revealed in this study. (*C*) p25 generation from p35, a neuron-specific TPKII/CDK5 activator, after 110 nM synthetic ASPD treatment (*Right*; representative Western blot). Data were normalized to actin and presented relative to total p35 and p25 amount at time 0. Mean ± SD; **P* < 0.02 compared with data at time 0 (Scheffé's post hoc test, *n* = 4~6). (*D*) TPKI/GSK3β activation as shown by phospho-Tyr^{216} increase and phospho-Ser^{9} decrease after 110 nM synthetic ASPD treatment (*Right*; representative Western blot). Data were normalized to total TPKI/GSK3β and presented relative to each phospho-protein amount at time 0. Mean ± SD; **P* < 0.002 compared with data at time 0 (Scheffé's post hoc test, *n* = 4~6). (*E*) Time-dependent increases in tau phosphorylation after 110 nM synthetic ASPD treatment. Data were normalized to total tau and presented relative to each phospho-protein amount at time 0. Vehicle controls are shown as inverted triangles in black for pSer^{396} and white for pSer^{404}. Mean ± SD; **P* < 0.0001 compared with data at time 0 (Scheffé's post hoc test, *n* = 3~4). (*F*) Time-dependent decreases in MAP2 and tau after 110 nM synthetic ASPD treatment (*Right*; representative Western blot). Data were normalized to actin and presented relative to each protein amount at time 0. Mean ± SD; **P* < 0.002 compared with data at time 0 (Scheffé's post hoc test, *n* = 4~6).

release from mitochondria through mitochondrial NCX and MPT pore opening (observed as the sharp increase $[Ca^{2+}]_i$), which results in the eventual death of neurons.

Previously we have shown involvement of tau protein kinase I/glycogen synthase kinase-3β (TPKI/GSK3β) in ASPD neurotoxicity (18). We also found that tau protein kinase II/cyclin-dependent protein kinase 5 (TPKII/CDK5) was activated after ASPD treatment (Fig. 5 *C* and *D*) and tau phosphorylation increased at Ser^{396} and Ser^{404}, which are known to be phosphorylated in AD brains by TPKI/GSK3β/TPKII/CDK5 and TPKII/CDK5, respectively (24) (Fig. 5*E*). Furthermore, tau and microtubule-associated protein 2 (MAP2) were rapidly lost after ASPD treatment (Fig. 5*F*). Tau phosphorylation and loss, together with MAP2 loss, could destabilize microtubules and promote neurodegeneration.

Next, time-lapse DIC images of mature neurons after ASPD treatment were taken. Because of osmotic imbalance, neurons started swelling at ~30 min after exposure to 140 nM synthetic ASPD, and cell shrinkage, a ubiquitous feature of apoptosis (25), took place in ~3–5 h (Fig. 6*A*, Fig. S4*A*, and Movie S1). Subsequently, DNA fragmentation became detectable after 5 h (Fig. 6*B*). Scanning electron microscopic (SEM) images clearly showed ASPD-induced neuronal swelling and shrinkage (Fig. 6*C*). The movie shows that the surface of the ASPD-treated neurons became rough within 30 min after the ASPD treatment (Movie S1) and holes appeared within 1 h (see arrows in Fig. 6*C*). Similar swelling and shrinkage of neurons were induced by 100 nM ouabain (Fig. 6*A*, Fig. S4*A*, and Movie S2), which selectively blocks rodent NAKα3 activity (26). Unlike ASPD and ouabain, staurosporine, an apoptosis inducer that inhibits multiple kinases, induced shrinkage but not swelling (Fig. 6*A*, Fig. S4*A*, and Movie S3). Vehicle treatment induced neither swelling nor shrinkage (Fig. 6*A*, Fig. S4*A*, and Movie S4). Ouabain also elicited the events triggered by ASPD (summarized in Fig. 5*B*; see also Fig. S3*F*). Our data are consistent with the conclusion that NAKα3 is a death target for ASPD toxicity. We summarize a possible ASPD-induced sequence of events leading to neuronal death in Fig. 6*A*.

We next examined NAKα3 localization in human brains. In nonclinically demented individual (NCI) cerebrum, punctate staining by anti-NAKα3 antibody surrounded the cell body of pyramidal neurons (arrows in Fig. 6*D*, *Upper Left*) and diffuse staining was detected on axons and in neuropils. Intense staining was found in basket cells surrounding Purkinje cells in NCI cerebellum (Fig. 6*D*, arrowheads, *Lower Left*). NAKα3 localization was consistent with that in adult mouse brain (27).

We found that NAKα3 staining was essentially lost in AD cerebrum, whereas it was not decreased in AD cerebellum (Fig. 6*D*, *Right*). Quantitative dot blotting with an ASPD-specific antibody, rpASD1, showed patient ASPD levels in NCI cerebrum, AD cerebrum, and AD cerebellum of 0.7 ± 0.4, 55.7 ± 7.0, and 0.7 ± 0.7 pmol/mg soluble brain extracts, respectively (a representative blot in Fig. 6*D*), suggesting that decreased NAKα3 staining correlated with patient ASPD levels in AD brains. Comparison of quantitative dot blotting results with rpASD1 and those with anti-Aβ antibody 82E1 indicated that patient ASPD

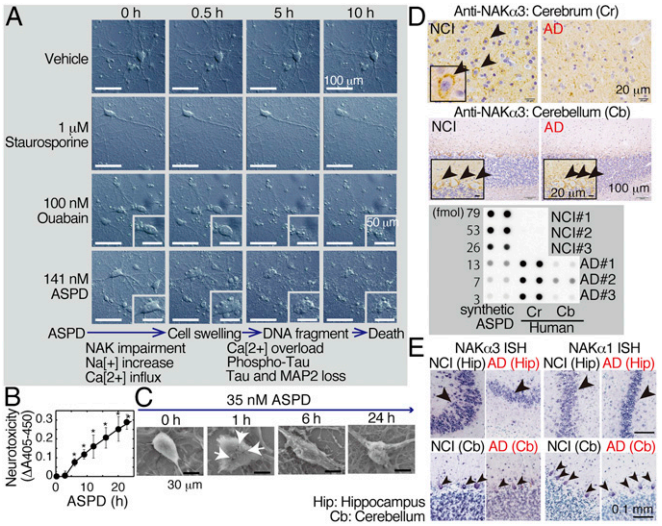

Fig. 6. ASPD effects on NAKα3-expressing neurons in rat neurons and human brains. (*A*) Representative time-lapse images of mature rat hippocampal neurons treated with each reagent (Movies S1–S4). (*B*) Time-dependent increase in apoptotic DNA fragmentation (determined as in Fig. 1*A*) induced by 140-nM synthetic ASPD. (*C*) SEM showed the surface and morphology of mature rat hippocampal neurons treated with 35 nM synthetic ASPD. (*D* and *E*) Immunohistochemical studies using anti-NAKα1 or anti-NAKα3 antibody on 4-μm paraffin-embedded sections in *D* and ISH analyses using probes for *ATP1A1* and *ATP1A3* on 10-μm paraffin-embedded sections in *E*. Soluble extracts were obtained from these brains and amounts of patient ASPD (representative blots in *D*) and Aβ in the extracts were determined by dot blotting as 429 ± 50 and 695 ± 104 (μg/g brain, $n = 3$), respectively.

accounted for 62 ± 3% ($n = 3$) of soluble Aβ. Unlike decreased NAKα3 staining, anti-NAKα1 antibody showed diffuse staining throughout NCI and AD cerebrum (Fig. S4*B*). Results of in situ hybridization (ISH) of adjacent sections of the same AD or NCI cases with NAKα3 mRNA (*ATP1A3*) or NAKα1 mRNA (*ATP1A1*) ($n = 3$ each) showed the same correlation with the histological data (compare Fig. 6*E* and Fig. S4*C* with Fig. 6*D* and Fig. S4*B*). With NAKα3 ISH, the signal intensity of *ATP1A3* was clearly lower in layers of pyramidal neurons in the hippocampus in AD compared with that observed in NCI. No obvious differences were detected in the cerebellum between AD and NCI. With NAKα1 ISH, the signal intensity of *ATP1A1* was not changed in both regions between AD and NCI cases. These results are consistent with a previous quantitative ISH study on AD patients (28) and suggest NAKα3-expressing neurons are preferentially lost in AD-susceptible brain regions where ASPD concentrations are high.

Structural Characteristics of ASPD and Their Target, Ex4 of NAKα3. To examine structural features of ASPD relevant to binding with NAKα3, we acquired solution NMR spectra of ^{15}N-labeled ASPD. Although we detected 39 heteronuclear single quantum coherence (HSQC) signals in the case of freshly dissolved Aβ, we detected 14 of 39 HSQC signals representing peptide backbones of Aβ in ASPD, and these were nearly superimposable on the signals of the $Aβ_{1–13}$, $Aβ_{15–16}$, and $Aβ_{23}$ regions of monomer (Fig. 7*A*). Remaining NMR-invisible amino acids presumably form a magnetically nonequivalent core. In other words, the NMR-visible amino acids, although derived from different Aβ regions, may exist in close proximity to form the ASPD surface (Fig. 7*B*), in accordance with our finding that specific binding of monoclonal mASD3 antibody to ASPD was blocked by pentapeptides covering $Aβ_{2–8}$, $Aβ_{15–19}$, or $Aβ_{19–23}$ (19). Because mASD3 antibody neutralizes ASPD toxicity (19), the NMR-identified ASPD surface is likely involved in binding to NAKα3. The HSQC spectra of ASPD were different from those of precursors of synaptotoxic dodecamers (termed globulomer) (29) and of LMW oligomers (30). Thus, ASPD appear to be structurally distinct from preglobulomers and LMW oligomers. This finding is consistent with our finding that ASPD are immunologically distinct from synaptotoxic oligomers (19). We obtained the same HSQC spectra of ASPD in all experiments ($n = 3$), suggesting that there is one defined structure that is dominant within the ASPD sample. Taken together with our previous immunological data using ASPD-specific antibodies (details in Table S1), this finding supports the notion that ASPD consist of closely related structures. Our recent analysis of ASPD structure using solid-state NMR also supports the notion (31).

The above findings suggest that the unique ASPD surface has a key role in ASPD-NAKα3 interaction. Because protein–protein interaction inhibitors can be designed based on the protein surface region essential for binding, we sought to determine which extracellular region of NAKα3 serves as the ASPD target site. NAKα1 and NAKα3 share 96% sequence identity. Given ASPD's preferential binding to NAKα3, the NAKα3-specific region, either the first extracellular loop (Ex1) or the fourth extracellular loop (Ex4) (Figs. 3*B* and 7*C*), would be the key ASPD target. We found that a chemically synthesized octapeptide from Ex4 (RLNWDDRT) significantly blocked ASPD toxicity, whereas Ex1 peptides neither bound to ASPD, as determined by SPR (Fig. S5*A*), nor blocked ASPD toxicity (Fig. 7*D*). Scrambled Ex4 peptides failed to block ASPD toxicity (Fig. 7*D*). We confirmed that Ex4 interfered with binding of both patient ASPD and synthetic ASPD to mature hippocampal neurons (Fig. 7*E* and Fig. S5*B*), in addition to blocking the subsequent $[Ca^{2+}]_i$ increases (Fig. S3D_4) and activation of the kinases (Fig. S5*C*). Notably, with 15-min patient ASPD treatment, neurites began to degenerate (Fig. 7*E*, arrowheads). This degeneration was almost completely blocked by Ex4 (Fig. 7*E*). These findings suggest that Ex4 is the main ASPD target site (pink in Fig. 7*C*).

We then planned to develop ASPD-binding peptides with toxicity-neutralizing activity by using phage display (PD) analysis. Three independent screenings of a randomized 12-mer peptide library detected ~21 kinds of ASPD-binding peptides with high His and Trp contents. Among them, many showed similarity to Ex4 of NAKα3. Chemically synthesized PD-identified dodecapeptides (PD2, -50, -68) bound to ASPD ($K_d = 5.8–8.9 \times 10^{-8}$ M by SPR). These dodecapeptides, which commonly contain a four-amino acid sequence (H*NW) similar to Ex4 (RLNW; corresponding to positions 877–880), inhibited ASPD toxicity toward mature neurons as effectively as the Ex4-derived peptide, whereas other peptides containing H**W (lacking NAKα3-specific Asn) were ineffective (Fig. 7*F*). Notably, ASPD-binding tetrapeptide PD2-11 (HFNW) was enough to significantly block binding and neurotoxicity of ASPD (Fig. 7*F* and Fig. S5*B*). These findings suggest that the NAKα3-specific region in Ex4 encompassing residues Asn^{879} and Trp^{880} is essential for ASPD–NAKα3 interaction (Fig. 7 *C* and *G*).

We built a 3D homology model of human NAKα3 based on the pig NAKα1 structure (32), as no crystal structure of human NAKα3 is available. Ex4 appeared to form a cavity and Asn^{879} and Trp^{880} are exposed on the NAKα3 surface, to which ASPD can gain access (Fig. 7*C*). Molecular modeling suggested that the mature NAK pump has a 9.9-nm-wide opening (Fig. S6). Solution atomic force microscopy showed that ASPD are 7.2 ± 2.6 nm in height (20). The maximum number concentration of bound ASPD, calculated from B_{max}, was 14 ± 0.7 pmol of ASPD per milligram of membrane protein (Fig. 1*C*). This concentration was 40% of the concentration of NAKα3 (35.2 ± 10 pmol/mg membrane protein; $n = 4$) that we measured (as shown in Fig. 3*G* using prequantified, cell-free synthesized NAKα3 as the quantification standard; for details see *SI Materials and Methods*) and it was ~37–88% of the concentrations found in the literature (16–38 pmol/mg membrane protein) (33, 34). Simple arithmetic calculations thus give an ASPD:NAKα3 ratio ranging from 1:1–1:3. However, because past

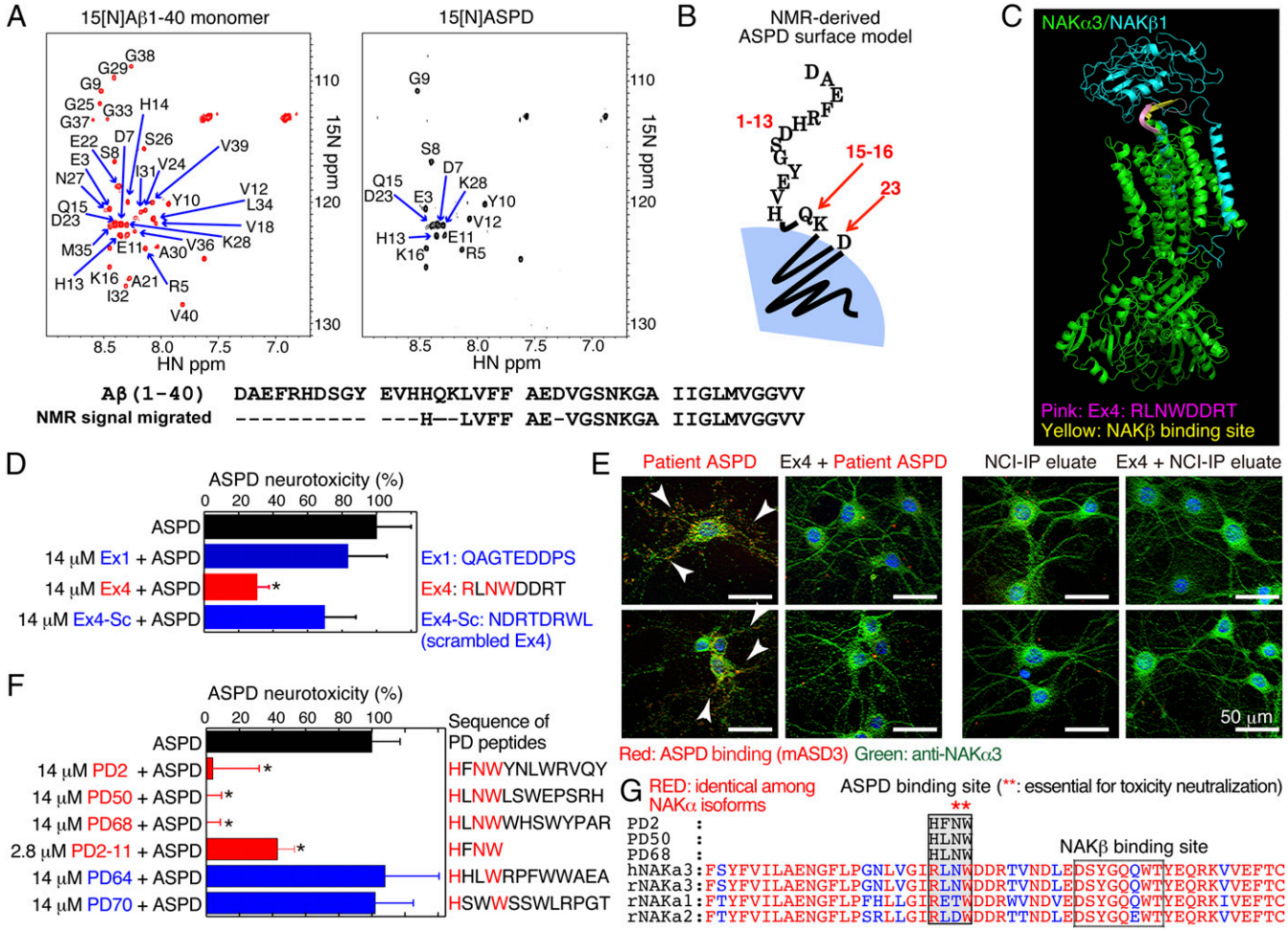

Fig. 7. Structural Basis For ASPD Binding To NAKα3. (*A*) ^{1}H-^{15}N HSQC spectra of ~350 nM ^{15}N-ASPD and ~100 μM ^{15}N-Aβ_{1-40} monomers in 0.5× PBS [supplemented with 5% (vol/vol) D_2O] were recorded at 298K on a 600-MHz Bruker *AVANCE*-III spectrometer equipped with a cryogenic TCI probe. (*B*) Schematic diagram of the NMR-derived ASPD surface. (*C*) A 3D homology model of human NAKα3 was constructed using the Prime program (Schrödinger) based on the structure of pig NAKα1 (32) as a template (PDB ID code 3B8E). (*D*) The effect of each NAKα3-derived Ex1, Ex4, or scrambled Ex4 peptides on 140 nM synthetic ASPD neurotoxicity was examined as in Fig. 1*A*. Mean ± SD; *$P < 0.001$ Scheffé's post hoc test, compared with vehicle, $n = 3$. (*E*) Representative *z*-stack images of 26 DIV hippocampal neurons, after 15-min treatment with 7 nM patient ASPD (immunoisolated from the patient extracts as in Fig. 2*B*), with or without 30-min pretreatment with Ex4 (20 μM in final concentration). IP eluates of NCI brain extracts, in which ASPD were not detected by dot blotting, were used as a control. ASPD-binding sites (red) and anti-NAKα3 staining (green) were detected as in Fig. 3*E*. (*F*) The effect of each Ex4-mimicking ASPD-binding peptides on 140 nM synthetic ASPD neurotoxicity. All peptides used here contained a free N-terminal amino group and a carboxylic acid at the C terminus. Mean ± SD; *$P < 0.001$ Scheffé's post hoc test, compared with vehicle, $n = 3$. (*G*) Alignment of Ex4 regions.

studies have shown that the NAK pump exists predominantly as $(NAK\alpha3)_2$:$(NAK\beta1)_2$ heterotetramer in membranes (35, 36) and ASPD appeared to bind almost all NAKα3-containing NAK pumps in membranes (Fig. 3*E*), we infer, using Occam's razor (37), that the most likely ratio is 1:2 (i.e., 1:1 binding of ASPD with NAKα3 dimer). This inference is consistent with other ASPD binding data (Fig. S6). Because the tetrapeptide segment in Ex4 of NAKα3 is conserved in rodents and humans (Fig. 7*G*), this opens up possibilities for knowledge-based design of inhibitors of neuronal death in AD.

Discussion

Past studies have reported the loss of the NAK pump activity, and the protein itself, in the brains of AD patients (28, 38, 39). In particular, NAKα3 expression, but not NAKα1 expression, is reduced in the frontal cortices of AD patients and this reduction correlates inversely with levels of diffuse plaques in that region (28). No such reduction is observed in the unaffected cerebellum of the same patients (28). NAKα3 activity was reported to decrease in Aβ_{1-40}-treated neuronal cultures (40) and the NAK pump activity was reported to decrease in 17- to 18-mo-old *APP* and *presenilin-1* transgenic mice (41). These previous observations suggest a potential link between Aβ and NAKα3 impairment. However, until now, the question of whether NAKα3 impairment is the cause or the result of neuronal death has remained unanswered. We present here direct evidence that the neuron-specific α-subunit of the NAK pump, NAKα3, is the neuronal death-inducing target of ASPD.

SPR data demonstrated direct binding of ASPD to NAKα3 (Fig. 3*F*). ASPD-binding to NAKα3 impaired rapidly NAKα3-specific NAK pump activity (Fig. 4*A*). Cytoplasmic Ca^{2+} overload was highly correlated with ASPD-binding (compare Figs. 1*C* and 4*D*), which eventually led to mitochondrial defects and neuronal death (Fig. 5*A*), as observed in AD (42). Stable knockout of NAKα3 expression with a microRNA-expressing virus vector decreased NAKα3-expressing neurons and abolished ASPD-binding and ASPD-induced neurodegeneration (Fig. 3*H*). ASPD binding peptides inhibited the ASPD binding to NAKα3 and protected

mature neurons from ASPD neurotoxicity (Fig. 7 *D–F*, and Figs. S3D_4 and S5 *B* and *C*). In addition to these cell-based data, we found that NAKα3-expressing neurons were lost in AD-susceptible regions, such as the cortex and the hippocampus in patients (where ASPD levels were high), but were not lost in the far less affected cerebellum of the same patients (where ASPD levels were low) (Fig. 6 *D* and *E* and Fig. S4 *B* and *C*). The explanation for these regional differences in ASPD concentrations must await further experimentation, but these observations further support our conclusion that NAKα3 serves as the specific death-inducing target of ASPD.

Recent studies have shown that Aβ forms numerous structurally distinct oligomers that may contribute differently to disease pathogenesis (6, 19). Aβ receptor/ligand systems may be organized into three categories (Fig. 8 and Table S3). The first category involves regulating the CNS concentration of Aβ monomer available for assembly. The second category involves Aβ impairment of synaptic connections by indirectly affecting NMDAR activity (see *SI Discussion* for more details about the first two categories). Postsynaptic Sigma-2/PGRMC1 (progesterone receptor membrane component 1) has been reported to serve as a receptor for 50~75 kDa $Aβ_{1–42}$ oligomers (43). We report here a third system involving presynaptic neurons. Presynaptic neuronal Ca^{2+} hyperactivation has been reported to occur near amyloid plaques in AD model mice (44). Interestingly, such hyperactivation of neurons in hippocampus has been associated with the cortical thinning in mild cognitive impairment patients and has been considered to be an early indicator of AD-related neurodegeneration (45). However, the underlying mechanisms were largely unknown. We have previously shown that ASPD colocalize with presynaptic Bassoon (19). Among different NAKα subunits, only NAKα3 is present in the presynaptic side of neurons (27, 46–48). Electrophysiological studies have also shown the importance of NAKα3 in the presynaptic function (49, 50). Our data are consistent with ASPD binding to presynaptic NAKα3 of mature neurons, leading to activation of presynaptic N-type VGCC, and eventual death of NAKα3-expressing neurons. Notably, NAKα3 appears as punctate patterns restricted to layers III and V of the neocortex (27), where N-type VGCC are present (51). These layers are particularly vulnerable in AD brains (52). It is an intriguing speculation that the 100-kDa band sometimes observed by Gong et al. in ligand overlay assays with ADDLs was NAKα3 (53).

The human NAKα3 gene *ATP1A3* is located on chromosome 19q13.31, an AD linkage region, but at present there are no reports that mutations in *ATP1A3* are linked to AD. The mutation rate in *ATP1A3* is very low in humans (54), suggesting that people with mutations in *ATP1A3* might be at high risk of neurodevelopmental/neuropsychiatric diseases and develop these diseases before they become old. Indeed, genetic studies have shown that mutations in the protein-coding region of *ATP1A3* cause rapid-onset dystonia parkinsonism, alternating hemiplegia of childhood, and cerebellar ataxia, areflexia, pes cavus, optic atrophy, and sensorineural hearing loss syndrome (54). Notably, although a direct linkage of *ATP1A3* mutations to AD is difficult to detect, AD and *ATP1A3*-mutated diseases share features such as convulsive seizures (derived from hyperactivity of neurons). A recent clinical study of AD patients has revealed that convulsive seizures occurred early in the course of AD, which often began around the same time when symptoms of neurodegeneration first appeared (55). Levetiracetam, which inhibits presynaptic calcium channels (56), suppresses neuronal hyperactivation, and reverses cognitive deficits in their AD model mice (57). These results are consistent with our findings (Fig. 8) and suggest that hyperactivation of presynaptic neurons occurs in AD patients contemporaneously with neurodegeneration.

AD is a progressive disease with risk highly correlated with aging. As shown in Fig. 2*A*, ASPD are not detectable in brains of most healthy old people, suggesting that accumulation of ASPD may not begin in the very early phase of Aβ accumulation. This notion is consistent with the fact that ASPD are minimally present in the brains of *APP*-overexpressing mice, which accumulate dodecamers and retain the early features of AD development (such as spine loss) but not the features of symptomatic human AD (such as neurodegeneration) (19). These observations suggested to us that formation of ASPD might require an age-related "facilitating factor," in addition to *APP* overexpression. A prospective study of ASPD formation relative to AD development and progression could be of interest. We think this study may be particularly significant in the light of our prior work showing that ASPD levels correlate with disease severity (19) and the data presented here (Fig. 2*A*) demonstrating that AD patient ASPD levels correlate with the severity of neurodegeneration based on Braak staging and duration of disease.

Fine structural analysis of ASPD by solution NMR suggests that amino acid residues Ala^{1}-His^{13}, Gln^{15}-Lys^{16}, and Asp^{23} are involved in forming a portion of the ASPD surface, a portion likely involved in NAKα3-binding (Fig. 7*B*). Furthermore, molecular modeling of NAKα3 indicated that the region in Ex4 of NAKα3 encompassing residues Asn^{879} and Trp^{880} is essential for the ASPD–NAKα3 interaction. Indeed, an ASPD-binding tetrapeptide that mimics this Ex4 region blocked ASPD neurotoxicity. Because Asn^{879} is essential for neutralizing ASPD neurotoxicity, we speculate that H-bonding interactions are involved in the ASPD–NAKα3 interaction. Interestingly, in the case of human NAKα2, mutation at this tryptophan (W887R; Trp^{887} in NAKα2 corresponds to Trp^{880} in NAKα3), which is highly conserved among all NAKα isoforms (Fig. 7*G*), leads to complete loss of catalytic activity and causes familial hemiplegic migraine type 2 (58). This finding suggests the importance of this conserved Trp for native NAKα function and it may be that ASPD binding to the region containing this Trp causes impairment of NAKα3 function.

Except for the NAKβ subunit and agrin, all other NAKα-binding proteins have been reported to bind to the intracellular region of NAKα (59). Because this NAKβ-binding region is located 10 amino acids more C-terminally than Trp^{880} (Fig. 7*G*), the Ex4-mimicking tetrapeptide is unlikely to interfere with the NAKα–NAKβ interaction. In the case of the NAKα2 mutation W887R, loss of NAK pump activity occurs without interfering with the NAKα–NAKβ interaction because the NAK pump containing the NAKα and NAKβ subunits is present at substantial levels in the plasma membrane (58). With respect to agrin, although its binding region in NAKα3 has not been

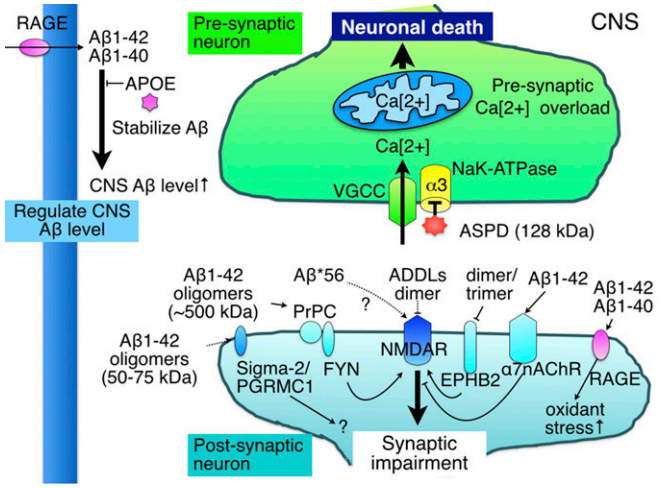

Fig. 8. Major Aβ ligand/receptor systems previously detected and the system identified in this work (Table S3).

determined, it has been suggested to take the place of NAKβ, and accordingly, it is reasonable to consider that agrin and NAKβ share the same binding region (59). Taken together, these observations suggest that peptidomimetics would not disrupt interactions between NAKα3 and proteins other than ASPD. The Ex4-mimicking tetrapeptide (PD2–11, MW602.6) that inhibits ASPD neurotoxicity is sufficiently small that the molecule could serve as a lead compound for knowledge-based design of peptidomimetics. This class of compounds is expected to offer superior stability and pharmacokinetics compared with anti-Aβ antibodies. Given the essential functions of the NAK pump in neurons (22), direct modulation of the NAK pump would be a risky approach. We therefore propose a new strategy to treat AD by blocking ASPD–NAKα3 interaction through masking the Aβ oligomer surface with specific peptidomimetics, as illustrated in Fig. S6. In summary, our data support the conclusion that ASPD–NAKα3 interaction is a cellular basis for neuronal loss induced by ASPD and that blocking this interaction could be a useful strategy for AD treatment.

Materials and Methods

Ethics. The Bioethics Committees and the Biosafety Committees of MITILS, Niigata University, Kyoto University, FBRI, and TAO approved experiments using human subjects. The Animal Care and Experimentation Committees of MITILS, Kyoto University, FBRI, and TAO approved animal experiments.

ASPD Preparation. ASPD are neurotoxic, spherical Aβ oligomers of 10- to 15-nm diameter (measured by TEM) that are recognized by ASPD-specific antibodies (19, 20). Patient ASPD were purified from the 100-kDa retentates of soluble AD brain extracts (devoid of LMW oligomers, prepared as in ref. 19) by immunoprecipitation (IP) using haASD1 (*SI Materials and Methods*). Synthetic ASPD were formed in 50 μM $Aβ_{1–42}$ solution (with or without 2 μM biotinylated $Aβ_{1–40}$) using in-house–prepared highly soluble Aβ peptides (essential for obtaining ASPD) (*SI Materials and Methods, Aβ synthesis*) in F12 buffer without L-glutamine and phenol red by slowly rotating the solution for ∼16 h at 4 °C (19). The level of $Aβ_{1–42}$-ASPD in this $Aβ_{1–42}$ solution after slow rotation is usually ∼30%. Synthetic ASPD were obtained in the fraction that passed through 0.22-μm filters, but was retained on 100-kDa MWCO filters (Sartorius) (19). ^{15}N-Labeled ASPD were prepared in the same way using purified *Escherichia coli*-expressed ^{15}N-labeled $Aβ_{1–40}$ (60). ASPD quality was confirmed by dot blotting, TEM, amino acid analysis, and toxicity assays (20).

Statistical Analyses. Statistical analysis was performed using StatView5.0 (SAS Institute).

Other Methods. Methods for Aβ synthesis, preparation of 20- to 30-nm Aβ aggregates, primary neuronal cultures, ASPD toxicity, ASPD binding, immunocytochemistry, microRNA of *ATP1A3*, Western and Far-Western blotting and MS/MS, cell-free NAKα3 production, SPR, IP, NAK activity, Ca^{2+} and Na^{+} imaging, time-lapse, dot blotting, TEM, SEM, Human brain pathology and ISH, glycerol gradient sedimentation, PD, NMR, and molecular modeling are described in *SI Materials and Methods*.

Supporting Information. Additional information can be found in *SI Materials and Methods, SI Discussion*, Figs. S1–S6, Tables S1–S3, and Movies S1–S4. Fig. S1 shows that glutamate receptor antagonists did not change ASPD neurotoxicity. Fig. S2 shows data on ASPD interactions with NAKα3, developmental changes in NAKα3 levels, coimmunoprecipitations, and immunostaining. Fig. S3 shows ASPD-induced Na^{+} increase, Ca^{2+} overload induced by different concentrations of ASPD, which were abolished by EGTA pretreatment, as well as ouabain-induced Ca^{2+} overload and tau phosphorylation/destabilization. Fig. S4 shows time-lapse shots and immunohistochemical studies of human brains using anti-NAKα1 antibody and ISH. Fig. S5 shows ASPD-binding peptides inhibit ASPD-binding to NAKα3 and other ASPD-induced downstream phenomena. Fig. S6 presents a model of ASPD-NAKα3 interactions and how masking the ASPD surface with specific masking peptides or peptidomimetics could be a new therapeutic strategy.

ACKNOWLEDGMENTS. We thank S. Kikuchi, Y. Matsumura, and K. Takatsuka for technical assistance; Masatoshi Takeichi and Shigenobu Yonemoto for help in using the transmission electron microscope instrument; and Dominic Walsh for comments. This work was supported by grants from the Ministry of Health, Labor and Welfare (Research on Nanotechnical Medical and Initiative for Accelerating Regulatory Science in Innovative Drug, Medical Device, and Regenerative Medicine); the Ministry of Education, Culture, Sports, Science and Technology [Grant-in-Aid for Scientific Research B and Grant-in-Aid for Scientific Research on Innovative Areas (Comprehensive Brain Science Network)]; the Collaborative Research Project of the Brain Research Institute, Niigata University; the Takeda Science Foundation (M. Hoshi); and National Institutes of Health Grants NS038328 and AG041295 (to D.B.T.).

1. Hardy J, Selkoe DJ (2002) The amyloid hypothesis of Alzheimer's disease: Progress and problems on the road to therapeutics. *Science* 297(5580):353–356.
2. Klein WL, Krafft GA, Finch CE (2001) Targeting small Aβ oligomers: The solution to an Alzheimer's disease conundrum? *Trends Neurosci* 24(4):219–224.
3. Walsh DM, Selkoe DJ (2007) Aβ oligomers—A decade of discovery. *J Neurochem* 101(5):1172–1184.
4. Roychaudhuri R, Yang M, Hoshi MM, Teplow DB (2009) Amyloid β-protein assembly and Alzheimer disease. *J Biol Chem* 284(8):4749–4753.
5. Chiti F, Dobson CM (2009) Amyloid formation by globular proteins under native conditions. *Nat Chem Biol* 5(1):15–22.
6. Benilova I, Karran E, De Strooper B (2012) The toxic Aβ oligomer and Alzheimer's disease: An emperor in need of clothes. *Nat Neurosci* 15(3):349–357.
7. Wang HY, et al. (2000) β-$Amyloid_{1-42}$ binds to α7 nicotinic acetylcholine receptor with high affinity. Implications for Alzheimer's disease pathology. *J Biol Chem* 275(8):5626–5632.
8. Yan SD, et al. (1996) RAGE and amyloid-β peptide neurotoxicity in Alzheimer's disease. *Nature* 382(6593):685–691.
9. Cissé M, et al. (2011) Reversing EphB2 depletion rescues cognitive functions in Alzheimer model. *Nature* 469(7328):47–52.
10. Laurén J, Gimbel DA, Nygaard HB, Gilbert JW, Strittmatter SM (2009) Cellular prion protein mediates impairment of synaptic plasticity by amyloid-β oligomers. *Nature* 457(7233):1128–1132.
11. Danysz W, Parsons CG (2012) Alzheimer's disease, β-amyloid, glutamate, NMDA receptors and memantine–searching for the connections. *Br J Pharmacol* 167(2):324–352.
12. Shankar GM, et al. (2008) Amyloid-β protein dimers isolated directly from Alzheimer's brains impair synaptic plasticity and memory. *Nat Med* 14(8):837–842.
13. O'Nuallain B, et al. (2010) Amyloid β-protein dimers rapidly form stable synaptotoxic protofibrils. *J Neurosci* 30(43):14411–14419.
14. Lesné S, et al. (2006) A specific amyloid-β protein assembly in the brain impairs memory. *Nature* 440(7082):352–357.
15. Lambert MP, et al. (1998) Diffusible, nonfibrillar ligands derived from Aβ1-42 are potent central nervous system neurotoxins. *Proc Natl Acad Sci USA* 95(11):6448–6453.
16. Lacor PN, et al. (2007) Aβ oligomer-induced aberrations in synapse composition, shape, and density provide a molecular basis for loss of connectivity in Alzheimer's disease. *J Neurosci* 27(4):796–807.
17. Weiner MW, et al. (2012) The Alzheimer's Disease Neuroimaging Initiative: A review of papers published since its inception. *Alzheimer Dement* 8(1, Suppl):S1–S68.
18. Hoshi M, et al. (2003) Spherical aggregates of β-amyloid (amylospheroid) show high neurotoxicity and activate tau protein kinase I/glycogen synthase kinase-3β. *Proc Natl Acad Sci USA* 100(11):6370–6375.
19. Noguchi A, et al. (2009) Isolation and characterization of patient-derived, toxic, high mass amyloid β-protein (Abeta) assembly from Alzheimer disease brains. *J Biol Chem* 284(47):32895–32905.
20. Matsumura S, et al. (2011) Two distinct amyloid β-protein (Aβ) assembly pathways leading to oligomers and fibrils identified by combined fluorescence correlation spectroscopy, morphology, and toxicity analyses. *J Biol Chem* 286(13):11555–11562.
21. Verret L, et al. (2012) Inhibitory interneuron deficit links altered network activity and cognitive dysfunction in Alzheimer model. *Cell* 149(3):708–721.
22. Blanco G, Mercer RW (1998) Isozymes of the Na-K-ATPase: Heterogeneity in structure, diversity in function. *Am J Physiol* 275(5 Pt 2):F633–F650.
23. Catterall WA, Few AP (2008) Calcium channel regulation and presynaptic plasticity. *Neuron* 59(6):882–901.
24. Yamaguchi H, et al. (1996) Preferential labeling of Alzheimer neurofibrillary tangles with antisera for tau protein kinase (TPK) I/glycogen synthase kinase-3 β and cyclin-dependent kinase 5, a component of TPK II. *Acta Neuropathol* 92(3):232–241.
25. Bortner CD, Cidlowski JA (2002) Apoptotic volume decrease and the incredible shrinking cell. *Cell Death Differ* 9(12):1307–1310.
26. O'Brien WJ, Lingrel JB, Wallick ET (1994) Ouabain binding kinetics of the rat alpha two and alpha three isoforms of the sodium-potassium adenosine triphosphate. *Arch Biochem Biophys* 310(1):32–39.
27. Bøttger P, et al. (2011) Distribution of Na/K-ATPase alpha 3 isoform, a sodium-potassium P-type pump associated with rapid-onset of dystonia parkinsonism (RDP) in the adult mouse brain. *J Comp Neurol* 519(2):376–404.
28. Chauhan NB, Lee JM, Siegel GJ (1997) Na,K-ATPase mRNA levels and plaque load in Alzheimer's disease. *J Mol Neurosci* 9(3):151–166.
29. Yu L, et al. (2009) Structural characterization of a soluble amyloid β-peptide oligomer. *Biochemistry* 48(9):1870–1877.
30. Yamaguchi T, Matsuzaki K, Hoshino M (2011) Transient formation of intermediate conformational states of amyloid-β peptide revealed by heteronuclear magnetic resonance spectroscopy. *FEBS Lett* 585(7):1097–1102.

31. Parthasarathy S, et al. (2015) Structural insight into an Alzheimer's brain-derived spherical assembly of amyloid β by solid-state NMR. *J Am Chem Soc* 137(20):6480–6483.
32. Morth JP, et al. (2007) Crystal structure of the sodium-potassium pump. *Nature* 450(7172):1043–1049.
33. Pylova SI, Majkowska J, Hilgier W, Kapuściński A, Albrecht J (1989) Rapid decrease of high affinity ouabain binding sites in hippocampal CA1 region following short-term global cerebral ischemia in rat. *Brain Res* 490(1):170–173.
34. Bignotto M, Benedito MA (2006) Repeated electroconvulsive shock induces changes in high-affinity [^{3}H]-ouabain binding to rat striatal membranes. *Neurochem Res* 31(4): 515–521.
35. Hayashi Y, Mimura K, Matsui H, Takagi T (1989) Minimum enzyme unit for Na^+/K^+-ATPase is the αβ-protomer. Determination by low-angle laser light scattering photometry coupled with high-performance gel chromatography for substantially simultaneous measurement of ATPase activity and molecular weight. *Biochim Biophys Acta* 983(2):217–229.
36. Antolovic R, et al. (1999) Affinity labelling with MgATP analogues reveals coexisting Na^+ and K^+ forms of the α-subunits of Na^+/K^+-ATPase. *Eur J Biochem* 261(1):181–189.
37. Courtney A, Courtney M (2008) Comments regarding "On the Nature Of Science". *Physics in Canada* 64(3):7–8.
38. Liguri G, et al. (1990) Changes in Na^+,K^+-ATPase, Ca^{2+}-ATPase and some soluble enzymes related to energy metabolism in brains of patients with Alzheimer's disease. *Neurosci Lett* 112(2-3):338–342.
39. Hattori N, et al. (1998) Cl^--ATPase and Na^+/K^+-ATPase activities in Alzheimer's disease brains. *Neurosci Lett* 254(3):141–144.
40. Mark RJ, Hensley K, Butterfield DA, Mattson MP (1995) Amyloid β-peptide impairs ion-motive ATPase activities: Evidence for a role in loss of neuronal Ca^{2+} homeostasis and cell death. *J Neurosci* 15(9):6239–6249.
41. Dickey CA, et al. (2005) Dysregulation of Na^+/K^+ ATPase by amyloid in APP+PS1 transgenic mice. *BMC Neurosci* 6:7.
42. Marambaud P, Dreses-Werringloer U, Vingtdeux V (2009) Calcium signaling in neurodegeneration. *Mol Neurodegener* 4:20.
43. Izzo NJ, et al. (2014) Alzheimer's therapeutics targeting amyloid beta 1-42 oligomers II: Sigma-2/PGRMC1 receptors mediate Abeta 42 oligomer binding and synaptotoxicity. *PLoS One* 9(11):e111899.
44. Busche MA, et al. (2008) Clusters of hyperactive neurons near amyloid plaques in a mouse model of Alzheimer's disease. *Science* 321(5896):1686–1689.
45. Putcha D, et al. (2011) Hippocampal hyperactivation associated with cortical thinning in Alzheimer's disease signature regions in non-demented elderly adults. *J Neurosci* 31(48):17680–17688.
46. McGrail KM, Phillips JM, Sweadner KJ (1991) Immunofluorescent localization of three Na,K-ATPase isozymes in the rat central nervous system: Both neurons and glia can express more than one Na,K-ATPase. *J Neurosci* 11(2):381–391.
47. Pietrini G, Matteoli M, Banker G, Caplan MJ (1992) Isoforms of the Na,K-ATPase are present in both axons and dendrites of hippocampal neurons in culture. *Proc Natl Acad Sci USA* 89(18):8414–8418.
48. Azarias G, et al. (2013) A specific and essential role for Na,K-ATPase α3 in neurons co-expressing α1 and α3. *J Biol Chem* 288(4):2734–2743.
49. Taruno A, Ohmori H, Kuba H (2012) Inhibition of presynaptic Na^+/K^+-ATPase reduces readily releasable pool size at the avian end-bulb of Held synapse. *Neurosci Res* 72(2): 117–128.
50. Kim JH, Sizov I, Dobretsov M, von Gersdorff H (2007) Presynaptic Ca^{2+} buffers control the strength of a fast post-tetanic hyperpolarization mediated by the α3 Na^+/K^+-ATPase. *Nat Neurosci* 10(2):196–205.
51. Chung YH, Shin C, Park KH, Cha CI (2000) Immunohistochemical study on the distribution of the voltage-gated calcium channel α_{1B} subunit in the mature rat brain. *Brain Res* 866(1-2):274–280.
52. Bussière T, et al. (2003) Progressive degeneration of nonphosphorylated neurofilament protein-enriched pyramidal neurons predicts cognitive impairment in Alzheimer's disease: Stereologic analysis of prefrontal cortex area 9. *J Comp Neurol* 463(3):281–302.
53. Gong Y, et al. (2003) Alzheimer's disease-affected brain: Presence of oligomeric Aβ ligands (ADDLs) suggests a molecular basis for reversible memory loss. *Proc Natl Acad Sci USA* 100(18):10417–10422.
54. Heinzen EL, et al.; ATP1A3 Working Group (2014) Distinct neurological disorders with ATP1A3 mutations. *Lancet Neurol* 13(5):503–514.
55. Vossel KA, et al. (2013) Seizures and epileptiform activity in the early stages of Alzheimer disease. *JAMA Neurol* 70(9):1158–1166.
56. Vogl C, Mochida S, Wolff C, Whalley BJ, Stephens GJ (2012) The synaptic vesicle glycoprotein 2A ligand levetiracetam inhibits presynaptic Ca^{2+} channels through an intracellular pathway. *Mol Pharmacol* 82(2):199–208.
57. Sanchez PE, et al. (2012) Levetiracetam suppresses neuronal network dysfunction and reverses synaptic and cognitive deficits in an Alzheimer's disease model. *Proc Natl Acad Sci USA* 109(42):E2895–E2903.
58. Koenderink JB, et al. (2005) Na,K-ATPase mutations in familial hemiplegic migraine lead to functional inactivation. *Biochim Biophys Acta* 1669(1):61–68.
59. Reinhard L, Tidow H, Clausen MJ, Nissen P (2013) Na^+,K^+-ATPase as a docking station: protein-protein complexes of the Na^+,K^+-ATPase. *Cell Mol Life Sci* 70(2):205–222.
60. Hiroaki H, Umetsu Y, Nabeshima Y, Hoshi M, Kohda D (2011) A simplified recipe for assigning amide NMR signals using combinatorial ^{14}N amino acid inverse-labeling. *J Struct Funct Genomics* 12(3):167–174.
61. Kolansky DM, Brines ML, Gilmore-Hebert M, Benz EJ, Jr (1992) The A2 isoform of rat Na^+,K^+-adenosine triphosphatase is active and exhibits high ouabain affinity when expressed in transfected fibroblasts. *FEBS Lett* 303(2-3):147–153.
62. Blanco G, Xie ZJ, Mercer RW (1993) Functional expression of the α2 and α3 isoforms of the Na,K-ATPase in baculovirus-infected insect cells. *Proc Natl Acad Sci USA* 90(5): 1824–1828.
63. Blanco G, Sánchez G, Mercer RW (1995) Comparison of the enzymatic properties of the Na,K-ATPase α3β1 and α3β2 isozymes. *Biochemistry* 34(31):9897–9903.
64. Takatsuka K, Ishii TM, Ohmori H (2005) A novel Ca^{2+} indicator protein using FRET and calpain-sensitive linker. *Biochem Biophys Res Commun* 336(1):316–323.
65. Nozawa A, et al. (2011) Production and partial purification of membrane proteins using a liposome-supplemented wheat cell-free translation system. *BMC Biotechnol* 11:35.
66. Kaiser L, et al. (2008) Efficient cell-free production of olfactory receptors: Detergent optimization, structure, and ligand binding analyses. *Proc Natl Acad Sci USA* 105(41): 15726–15731.
67. Gill SC, von Hippel PH (1989) Calculation of protein extinction coefficients from amino acid sequence data. *Anal Biochem* 182(2):319–326.
68. Braak H, Alafuzoff I, Arzberger T, Kretzschmar H, Del Tredici K (2006) Staging of Alzheimer disease-associated neurofibrillary pathology using paraffin sections and immunocytochemistry. *Acta Neuropathol* 112(4):389–404.
69. Delaglio F, et al. (1995) NMRPipe: A multidimensional spectral processing system based on UNIX pipes. *J Biomol NMR* 6(3):277–293.
70. Hou L, Zagorski MG (2006) NMR reveals anomalous copper(II) binding to the amyloid Aβ peptide of Alzheimer's disease. *J Am Chem Soc* 128(29):9260–9261.
71. Gunter TE, Yule DI, Gunter KK, Eliseev RA, Salter JD (2004) Calcium and mitochondria. *FEBS Lett* 567(1):96–102.
72. Doczi J, et al. (2011) Complex contribution of cyclophilin D to Ca^{2+}-induced permeability transition in brain mitochondria, with relation to the bioenergetic state. *J Biol Chem* 286(8):6345–6353.
73. Deane R, et al. (2012) A multimodal RAGE-specific inhibitor reduces amyloid β-mediated brain disorder in a mouse model of Alzheimer disease. *J Clin Invest* 122(4): 1377–1392.
74. Deroo S, et al. (2015) Chemical cross-linking/mass spectrometry maps the amyloid β peptide binding region on both apolipoprotein E domains. *ACS Chem Biol* 10(4): 1010–1016.
75. Yamauchi K, et al. (1999) Higher avidity binding of apolipoprotein (E-AII) complex than of apolipoprotein E monomer to β-amyloid. *J Neurosci Res* 58(2):301–307.
76. Snyder EM, et al. (2005) Regulation of NMDA receptor trafficking by amyloid-β. *Nat Neurosci* 8(8):1051–1058.
77. Um JW, et al. (2012) Alzheimer amyloid-β oligomer bound to postsynaptic prion protein activates Fyn to impair neurons. *Nat Neurosci* 15(9):1227–1235.
78. Huang Y, Mahley RW (2014) Apolipoprotein E: Structure and function in lipid metabolism, neurobiology, and Alzheimer's diseases. *Neurobiol Dis* 72(Pt A):3–12.
79. Um JW, Strittmatter SM (2013) Amyloid-β induced signaling by cellular prion protein and Fyn kinase in Alzheimer disease. *Prion* 7(1):37–41.
80. Yan SS, et al. (2012) RAGE is a key cellular target for Abeta-induced perturbation in Alzheimer's disease. *Front Biosci (Schol Ed)* 4(4):240–250.
81. Parri HR, Hernandez CM, Dineley KT (2011) Research update: Alpha7 nicotinic acetylcholine receptor mechanisms in Alzheimer's disease. *Biochem Pharmacol* 82(8): 931–942.
82. Decker H, et al. (2010) N-methyl-D-aspartate receptors are required for synaptic targeting of Alzheimer's toxic amyloid-β peptide oligomers. *J Neurochem* 115(6): 1520–1529.